Available online at www.sciencedirect.com
ScienceDirect
Thin Solid Films 516 (2008) 4159–4167
www.elsevier.com/locate/tsf

Effect of polarization and morphology on the optical properties of absorbing nanoporous thin films

Ashcon Navid, Laurent Pilon *

Mechanical and Aerospace Engineering Department, Henry Samueli School of Engineering and Applied Science, University of California, Los Angeles, Los Angeles, CA 90095, USA

Received 23 May 2007; received in revised form 8 October 2007; accepted 30 October 2007
Available online 11 December 2007

Abstract

This paper investigates the possibility of tuning the optical properties of thin films by introducing nanopores with different shape, size, and spatial distribution. The complex index of refraction of nanoporous thin films with various morphologies is determined for normally incident transverse magnetic (TM) and transverse electric (TE) absorbing electromagnetic waves by numerically solving the two-dimensional Maxwell's equations. The numerical results are compared with predictions from widely used effective medium approximations. For thin films with isotropic morphology exposed to TM waves, good agreement is found with the parallel model. For thin films with anisotropic morphology, the numerical results for TE waves are independent of the morphology and agree well with the Volume Averaging Theory model. By contrast, for incident TM waves, the retrieved effective optical properties depend on both porosity and film morphology. These results can be used to design nanocomposite materials with tunable optical properties and to determine their porosity and pore's spatial arrangement.

Keywords: Mesoporous; Nanoporous; Optical materials; Nanostructure; Polarization; Optoelectronic devices; Dielectric constant; Waveguides

1. Introduction

Nanoporous thin films have been studied extensively in recent years [1–4]. Potential applications include dye-sensitized solar cells [5–7], low-k dielectric materials [8,9], thermal barrier coatings [10], catalysts [11], biosensors [12–14], and optical devices such as waveguides [15–17], Bragg reflectors, and Fabry–Perot filters [18–24]. In all the above applications, understanding and predicting the effects of porosity as well as pore shape, size, and spatial arrangement on optical properties of nanoporous materials are essential for optimizing device performance. Mesoporous silica thin films with cylindrical nanopores and controlled inter-pore spacing can be synthesized by calcinations of self-assembled surfactant micelles in a silica precursor matrix as reported by Alberius et al. [3] among others. Fig. 1 depicts a transmission electron microscopy (TEM) image of the resulting hexagonal mesoporous silica thin film synthesized in our laboratory with an inset clarifying the geometry and dimensions. The pores are 4.12 nm in diameter, with inter-pore spacing of 4.82 nm, and porosity estimated at 0.68.

Various effective medium approximations (EMA) have been proposed to treat heterogeneous media as homogeneous with some effective properties. The Maxwell–Garnett Theory (MGT) [25] models the effective relative electrical permittivity $\varepsilon_{r,eff}$ of heterogeneous media consisting of monodispersed metallic spheres in glass. The spheres are arranged in a cubic lattice structure within a continuous matrix and their diameter is much smaller than the wavelength of the incident electromagnetic (EM) wave. Then, $\varepsilon_{r,eff}$ is expressed as,

$$\varepsilon_{r,eff} = \varepsilon_{r,c}\left[1 - \frac{3\phi\left(\varepsilon_{r,c} - \varepsilon_{r,d}\right)}{2\varepsilon_{r,c} + \varepsilon_{r,d} + \phi\left(\varepsilon_{r,c} - \varepsilon_{r,d}\right)}\right] \quad (1)$$

where $\varepsilon_{r,c}$ and $\varepsilon_{r,d}$ are the dielectric constant of the continuous and dispersed phases, respectively, and ϕ is the volume fraction occupied by the dispersed phase. The MGT is not valid for porosities greater than 52% since spheres begin to overlap. However, it has been extensively used to determine effective properties over the full range of porosities [26–30]. In addition, for non-conducting particles, such as the dielectric spheres or

* Corresponding author. Tel.: +1 310 206 5598; fax: +1 310 206 4830.
E-mail address: pilon@seas.ucla.edu (L. Pilon).

0040-6090/$ - see front matter © 2007 Elsevier B.V. All rights reserved.
doi:10.1016/j.tsf.2007.10.117

cylinders, Eq. (1) is not valid. Nonetheless, it has been used for non-conducting dispersed phase materials, non-spherical geometries, and to model properties other than the effective dielectric constant [28,29]. More recently, Grimvall [31] attempted to account for non-spherical geometry through modification of the MGT. Unfortunately, such a model is involved and/or requires specific knowledge of the shape and orientation of the dispersed phase.

The series and parallel models are examples of two other commonly used models for predicting the effective electrical dielectric constant [32,33], index of refraction [28,34], and both thermal [10] and electrical conductivities [35] of two-phase media. The parallel model states that the effective property ψ_{eff} is a linear combination of the continuous and dispersed phases, i.e.,

$$\psi_{\text{eff}} = (1-\phi)\psi_{\text{c}} + \phi\psi_{\text{d}} \tag{2}$$

whereas the series model gives

$$\frac{1}{\psi_{\text{eff}}} = \frac{1-\phi}{\psi_{\text{c}}} + \frac{\phi}{\psi_{\text{d}}} \tag{3}$$

On the other hand, the reciprocity theorem models the effective property as [36],

$$\psi_{\text{eff}} = \psi_{\text{c}} \frac{1+\phi\left(\sqrt{\psi_{\text{c}}/\psi_{\text{d}}}-1\right)}{1+\phi\left(\sqrt{\psi_{\text{d}}/\psi_{\text{c}}}-1\right)} \tag{4}$$

Alternatively, applying the Volume Averaging Theory (VAT) to Maxwell's equations for arbitrarily shaped domains in a continuous matrix predicts the effective dielectric constant and effective electrical conductivity of a two-phase mixture as [37,38],

$$\varepsilon_{\text{r,eff}} = (1-\phi)\varepsilon_{\text{r,c}} + \phi\varepsilon_{\text{r,d}} \tag{5}$$

$$\sigma_{\text{eff}} = (1-\phi)\sigma_{\text{c}} + \phi\sigma_{\text{d}} \tag{6}$$

where σ_{c} and σ_{d} are the electrical conductivity of the continuous and dispersed phases, respectively. The authors discuss the validity of these expressions in depth, and state a set of inequalities to be satisfied [37,38]. Garahan et al. [39] used Eqs. (5) and (6) to derive the effective refraction and absorption indices of a two-phase nanocomposite material as,

$$n_{\text{eff}}^2 = \frac{1}{2}\left[A + \sqrt{A^2+B^2}\right] \quad \text{and} \quad k_{\text{eff}}^2 = \frac{1}{2}\left[-A + \sqrt{A^2+B^2}\right] \tag{7}$$

where

$$A = \varepsilon_{\text{r,eff}} = \phi\left(n_{\text{d}}^2 - k_{\text{d}}^2\right) + (1-\phi)\left(n_{\text{c}}^2 - k_{\text{c}}^2\right) \tag{8}$$

and

$$B = \frac{\lambda\sigma_{\text{eff}}}{2\pi c_0 \varepsilon_0} = 2n_{\text{d}}k_{\text{d}}\phi + 2n_{\text{c}}k_{\text{c}}(1-\phi) \tag{9}$$

Here, n and k respectively refer to the index of refraction and absorption index of the continuous phase (subscript c) and of the dispersed phase (subscript d). Unlike the other models, the VAT model for n_{eff} and k_{eff} depends on the porosity ϕ and on the real and imaginary parts of the complex index of refraction ($m=n-ik$) of both the dispersed and continuous phases, i.e., $n_{\text{eff}}=n(\phi, n_{\text{c}}, k_{\text{c}}, n_{\text{d}}, k_{\text{d}})$ [39]. In the limiting case of non-absorbing composite thin films (i.e., $k_{\text{eff}}=k_{\text{c}}=k_{\text{d}}=0$), the VAT model reduces to the Drude model given by $n_{\text{eff}}^2=\phi n_{\text{d}}^2+(1-\phi)n_{\text{c}}^2$ [40]. Note that the above mentioned EMA do not account for the polarization of the incident EM waves describing the direction of the electric field with respect to the plane of incidence defined by the Poynting vector and the normal vector of the surface on which it is incident. In transverse electric (TE) plane waves, the electric field is perpendicular to the plane of incidence while it is in that plane for transverse magnetic (TM) plane waves. Any arbitrary plane wave can be described as some combination of TE and TM waves. For a dense homogeneous film, the normal vector of the surface and the Poynting vector are collinear such that the plane of incidence and hence polarization cannot be defined. For a heterogeneous film such as that shown in Figs. 1 and 2, the surface is cylindrical such that the normal vector is no longer collinear with the Poynting vector allowing polarization to be defined that causes changes in transmittance and reflectance.

Experimental data for the effective dielectric constant and index of refraction of nanoporous media reported in the literature for various materials, morphologies, porosities, and pore sizes proves inconclusive for determining the best effective medium model. For example, data reported by Loni et al. [15] for the effective index of refraction of porous silicon, agrees with the MGT model while data from Labbe–Lavigne et al. [28] for the same material falls between the VAT and parallel models. Data for the effective dielectric constant of aerogels – an open-cell mesoporous SiO_2 thin film – measured by Hrubesh et al. [33] follows the parallel model while data reported by Si et al. [32] for

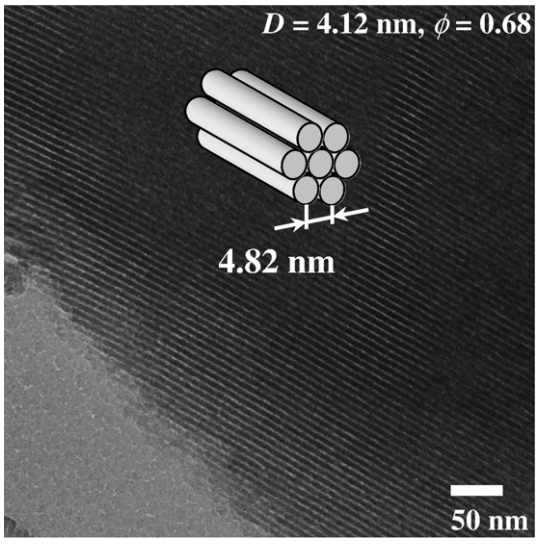

Fig. 1. Transmission electron microscopy (TEM) image of hexagonal mesoporous silica thin films with pore diameter D=4.12 nm and porosity ϕ=0.68.

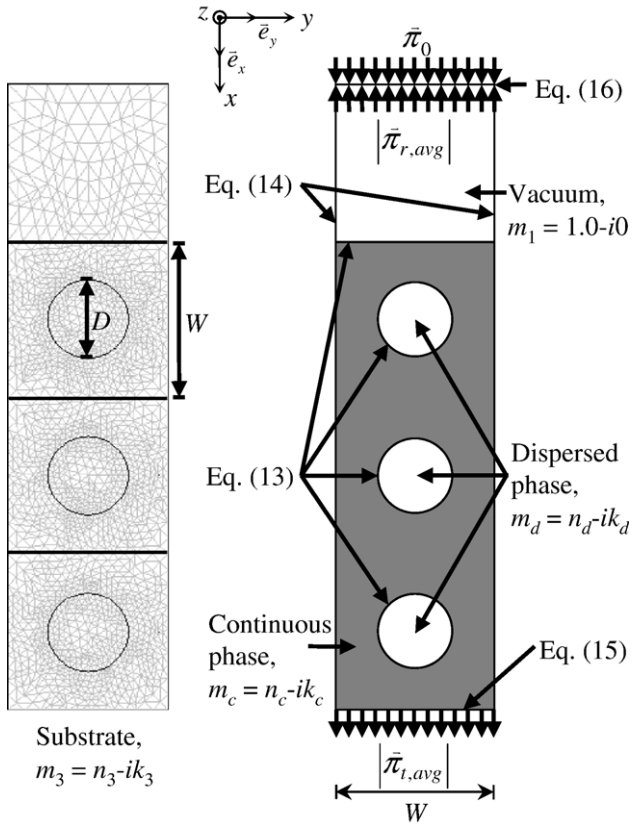

Fig. 2. Schematic of the physical model for the absorbing nanocomposite thin film, graphically depicting the location of the boundary conditions and the finite element mesh. Here, $\phi=0.1963$ and $L/D=6$. Note that actual computations are performed for $L/D\geq 150$, different porosities and pore spatial arrangement.

closed-cell morphology SiO_2 thin films are best described by the series model. Given the considerable contradictions among experimental studies noted above, a numerical approach is considered to assess the validity of the EMA.

Furthermore, For TE plane waves incident on a nanocomposite thin film, the effective index of refraction n_{eff} and the effective absorption index k_{eff} determined from the VAT model agree well with the numerical predictions of transmittance and reflectance for non-absorbing [41] and absorbing [39] media while the other models underpredict the numerical results. The results were obtained for normally incident TE EM plane waves traveling through (i) dielectric matrix with metallic nanowires as well as (ii) nanoporous silicon dioxide (SiO_2) and (iii) titanium dioxide (TiO_2) thin films consisting of aligned and equally spaced cylindrical nanopores or nanowires with various diameter D, film thickness L, porosity ϕ, and spatial distribution. Moreover, for thick enough films $L/D\geq 150$, the effective index of refraction depends only on porosity and on the optical properties of the two constitutive phases [39,41]. In other words, the effective optical properties do not depend on pore shape, size, and spatial distribution [41].

The present study investigates the effective index of refraction n_{eff} and the effective absorption index k_{eff} of nanoporous thin films with isotropic and anisotropic morphology comprised of horizontally aligned cylindrical nanopores with varying diameters and porosities for incident TM plane waves. Maxwell's equations are solved numerically to determine the spectral normal-normal transmittance and reflectance, from which, the effective index of refraction n_{eff} and the effective absorption index k_{eff} can be retrieved. In addition, comparisons are made with (i) various EMA and (ii) results obtained from TE plane waves [39]. This study is limited to non-magnetic materials whose relative magnetic permeability, μ_r, is unity, i.e., $\mu_{r,c}=\mu_{r,d}=\mu_{r,\text{eff}}=1$.

2. Analysis

2.1. Governing equations and numerical implementation

Fig. 2 illustrates the physical model of the nanocomposite thin film, along with the associated coordinate system, boundary conditions, and finite element grid. The model corresponds to a nanoporous thin film with three cylindrical pores with diameter $D=10$ nm and cubic cell width W of 20 nm corresponding to a porosity $\phi=\pi D^2/4W^2=0.1963$. Note that the model in Fig. 2 is illustrative only with three pores i.e., $L/D=6$. However, actual numerical computations are performed for a much larger number of pores ($L/D\geq 150$), different porosities, and varying pore spatial arrangement. Both continuous ($m_c=n_c-ik_c$) and dispersed ($m_d=n_d-ik_d$) phases are assumed to be homogenous and isotropic and to have the same optical properties as the bulk material. The thin film is deposited onto a non-absorbing dense substrate (medium 3, n_3, $k_3=0$) and surrounded by vacuum (medium 1, $n_1=1.0$, $k_1=0$). The nanocomposite thin film is treated as homogeneous (medium 2) with some effective optical properties n_{eff} and k_{eff}. A linearly polarized plane wave in TM mode is incident normal to the top surface of the absorbing thin film and travels in the x-direction through the two-dimensional thin film with the following general time-harmonic form,

$$\vec{H}(x,y,t) = H_z(x,y)e^{i\omega t}\vec{e}_z \quad \text{and} \qquad (10)$$
$$\vec{E}(x,y,t) = \left[E_x(x,y)\vec{e}_x + E_y(x,y)\vec{e}_y\right]e^{i\omega t}$$

where $\vec{H}$ is the magnetic field vector, $\vec{E}$ is the electric field vector while $\vec{e}_x$, $\vec{e}_y$, and $\vec{e}_z$ are the unit vectors, and $\omega=2\pi c_0/\lambda$ is the angular frequency of the wave. Maxwell's equations for general time-varying fields in a conducting medium are given by [42],

$$\nabla\times\left[\frac{1}{\mu_r\mu_0}\nabla\times\vec{E}(x,y,t)\right]-\omega^2\varepsilon_r^*\varepsilon_0\,\vec{E}(x,y,t)=0 \qquad (11)$$

$$\nabla\times\left[\frac{1}{\varepsilon_r^*\varepsilon_0}\nabla\times\vec{H}(x,y,t)\right]-\omega^2\mu_r\mu_0\,\vec{H}(x,y,t)=0 \qquad (12)$$

where μ_0 is the magnetic permeability of vacuum, μ_r is the relative magnetic permeability, and $\varepsilon_r^*=m^2=n^2-k^2-i2nk$ is the

complex dielectric constant. Maxwell's equations for TM waves are subject to the following boundary conditions,

$$\vec{n}\times\left(\vec{E}_1-\vec{E}_2\right)=\vec{0} \tag{13}$$

at dispersed − continuous phase interfaces,

$$\vec{n}\times\vec{E}=\vec{0} \tag{14}$$

at symmetry boundaries,

$$\sqrt{\mu_r\mu_0}\,\vec{H}-\sqrt{\varepsilon_0\varepsilon_r^*}\left(\vec{n}\times\vec{E}\right)=\vec{0} \tag{15}$$

at the film − substrate interface

$$\sqrt{\varepsilon_0\varepsilon_r^*}\left(\vec{n}\times\vec{E}\right)-\sqrt{\mu_0\mu_r}\,\vec{H}=-2\sqrt{\mu_0\mu_r}\,\vec{H}_0 \tag{16}$$

at the source surface

where $\vec{n}$ is the normal vector to the appropriate interface, $\vec{E}_1$ and $\vec{E}_2$ represent the electric fields in the surroundings and in the film, respectively, and $\vec{H}_0 = H_0\,\vec{e}_z$ is the incident magnetic field specified at the source surface (top surface of medium 1). Eq. (13) is used at all continuous/dispersed phase interfaces including the thin film top surface and the matrix/pore interfaces. Finally, it is important to note that Maxwell's equations are generally applied to macroscopic averages of the fields which can vary widely in the vicinity of individual atoms where they undergo quantum mechanical effects.

Moreover, the energy flux of the EM wave corresponds to the magnitude of the Poynting vector $\vec{\pi}$, defined as, $\vec{\pi}=\vec{E}\times\vec{H}$ [42]. The x-component of the time-averaged Poynting vector at a given point in space (x, y) averaged over the period $2\pi/\omega$ for the time-harmonic field is, $|\pi_x|_{\text{avg}}(x,y)=\frac{1}{2}\text{Re}\left\{\vec{E}\times\vec{H}^*\right\}$ [42], where $\vec{H}^*$ is the complex conjugate of $\vec{H}$ given by Eq. (10). The numerically calculated transmittance T_{num} is determined by dividing the value of the x-component of the Poynting vector averaged along the film-substrate interface and denoted by $|\pi_{x,t}|_{\text{avg}}$ by the incident average Poynting vector $|\pi_{x,0}|_{\text{avg}}$, i.e., $T_{\text{num}}=|\pi_{x,t}|_{\text{avg}}/|\pi_{x,0}|_{\text{avg}}$. Likewise, the numerically retrieved reflectance R_{num} is computed by taking the ratio of the x-component of the Poynting vector averaged along the top boundary of the film denoted by $|\pi_{x,r}|_{\text{avg}}$ to the incident average Poynting vector, i.e., $R_{\text{num}}=|\pi_{x,r}|_{\text{avg}}/|\pi_{x,0}|_{\text{avg}}$.

Finally, FEMLAB 3.1 was used to numerically solve Maxwell's equations in two-dimensions in the frequency domain for a TM incident wave applying the Galerkin finite element method on unstructured meshes.

2.2. Retrieval of effective complex index of refraction

The effective complex index of refraction is retrieved by minimizing the root mean square of the relative error for transmittance δT and reflectance δR given as,

$$\delta T^2=\frac{1}{N}\sum_{i=1}^{N}\left[\frac{T_{\text{th}}(\lambda_i)-T_{\text{num}}(\lambda_i)}{T_{\text{th}}(\lambda_i)}\right]^2 \quad \text{and} \tag{17}$$

$$\delta R^2=\frac{1}{N}\sum_{i=1}^{N}\left[\frac{R_{\text{th}}(\lambda_i)-R_{\text{num}}(\lambda_i)}{R_{\text{th}}(\lambda_i)}\right]^2$$

where $T_{\text{th}}(\lambda_i)$ and $R_{\text{th}}(\lambda_i)$ correspond to EM wave theory predictions at N different incident wavelengths λ_i. The theoretical transmittance and reflectance for a homogeneous and isotropic thin film (medium 2) on a solid substrate (medium 3) surrounded by air (medium 1) can be expressed as [42],

$$T_{\text{th}}(\lambda)=\frac{\tau_{12}\tau_{23}e^{-\kappa_2 L}}{1+2r_{12}r_{23}e^{-\kappa_2 L}\cos(\delta_{12}+\delta_{23}-\zeta_2)+r_{12}^2r_{23}^2e^{-2\kappa_2 L}} \tag{18}$$

$$R_{\text{th}}(\lambda)=\frac{r_{12}^2+2r_{12}r_{23}e^{-\kappa_2 L}\cos(\delta_{12}-\delta_{23}+\zeta_2)+r_{23}^2e^{-2\kappa_2 L}}{1+2r_{12}r_{23}e^{-\kappa_2 L}\cos(\delta_{12}+\delta_{23}-\zeta_2)+r_{12}^2r_{23}^2e^{-2\kappa_2 L}} \tag{19}$$

where

$$r_{ij}^2=\frac{\left(n_i-n_j\right)^2+\left(k_i-k_j\right)^2}{\left(n_i+n_j\right)^2+\left(k_i+k_j\right)^2},\quad \tau_{ij}=\frac{n_i}{n_j}\frac{4\left(n_i^2+k_i^2\right)}{\left(n_i+n_j\right)^2+\left(k_i+k_j\right)^2}$$
$$\tan\delta_{ij}=\frac{2\left(n_ik_j-n_jk_i\right)}{n_i^2+k_i^2-\left(n_j^2+k_j^2\right)},\quad \kappa_2=4\pi k_2/\lambda,\ \text{and}\ \zeta_2=4\pi n_2L/\lambda \tag{20}$$

The Microsoft Excel Solver was utilized in finding the optimum effective index of refraction n_{eff} and effective absorption index k_{eff} by minimizing δR and δT given by Eq. (17). Note that these equations are valid provided that (i) all interfaces are optically smooth, (ii) non-linear optical effects, and (iii) surface waves can be ignored. This is the case in this study.

Moreover, scattering of the EM wave by the pores is negligible since the size parameter $\chi=\pi D/\lambda$ in the present study varies between 0.003 and 0.079, i.e., $\chi<<1$. In other words, the nanoporous thin films considered in the presented study are treated as homogeneous and non-scattering. These assumptions have been verified quantitatively using the numerical results and will be discussed after validating the numerical procedure. For qualitative arguments, it is instructive to consider the well-known limiting case of a spherical scatterer in a non-absorbing medium such that $\chi<<1$. Then, Rayleigh scattering prevails and the scattering and absorption efficiency factors denoted by $Q_{\text{sca}}(\chi)$ and $Q_{\text{abs}}(\chi)$ are proportional to χ^4 and χ, respectively so that $Q_{\text{abs}}>>Q_{\text{sca}}$ [42,43]. In addition, Yin and Pilon [44] showed that for a non-absorbing spherical bubble ($m_{\text{d}}=1.0$) with size parameter $\chi<<1$ embedded in an absorbing matrix ($m_{\text{c}}=1.34-i0.01$), the absorption and scattering efficiency factors predicted by far field or near field approximations accounting for absorption by the surrounding medium are nearly identical to those predicted by the conventional Mie theory.

2.3. Validation of the numerical procedure and retrieval method

The numerical model was validated with a dense homogenous thin film ($n_2=1.4$, k_2) deposited on a non-absorbing silicon substrate ($n_3=3.39$, $k_3=0$) in air ($n_1=1.0$, $k_1=0$). The normal transmittance and reflectance were computed as a

function of wavelength between 400 and 900 nm for both a non-absorbing ($k_2=0$) and absorbing ($k_2=0.01$) thin film of thickness $L=2.0$ μm. The numerical results for transmittance and reflectance agree with theoretical predictions from Eqs. (18) and (19). For the non-absorbing thin film, the maximum relative difference between the theoretical and numerical transmittance and reflectance was 0.3% and 0.021%, respectively while for the absorbing thin film, the maximum relative difference was 0.1% and 1.1%, respectively. Note also that, under normal incidence, the transmittance and reflectance of a homogeneous and isotropic thin film are identical for TE and TM incident waves. Indeed, the plane of incidence and therefore polarization cannot be defined when the normal vector and the incident Poynting vector are collinear. This was verified numerically as a way to further validate the numerical procedure.

Validation of the retrieval method was performed for the same films. For the absorbing thin film, the inverse method returned the effective index of refraction $n_{\text{eff}}=1.39996$ and the effective absorption index $k_{\text{eff}}=0.00994$ which are within 2.9×10^{-3}% and 0.6% of the input values, respectively while for the non-absorbing thin film, $n_{\text{eff}}=1.39998$ fell within 1.1×10^{-3}% of the input value. Therefore, the numerical simulation and the above inverse method can be used to determine the effective complex index of refraction for nanocomposite thin films for TM polarization.

Finally, the assumption that scattering by the pores is negligible was numerically validated for all simulations. First, for a given thin film, the x-component of the Poynting vector along the film-substrate interface $|\pi_{x,t}|$ is always within 3% of its average value $|\pi_{x,t}|_{\text{avg}}$. In addition, the amplitude of the y-component of the time-averaged Poynting vector averaged along the film-substrate interface, is negligible compared with its x-component as the ratio $|\pi_{y,t}|_{\text{avg}}/|\pi_{x,t}|_{\text{avg}}$ is between 2.4×10^{-3} and 5.6×10^{-2}. In other words, it is established numerically that $|\pi_{x,t}|_{\text{avg}}>>|\pi_{y,t}|_{\text{avg}}$.

3. Results and discussion

3.1. EMA for TM waves

First, the effect of film thickness L on the effective complex index of refraction was considered for an imaginary nanoporous thin film with $n_c=4.0$, $k_c=0.01$, $n_d=1.0$, and $k_d=0$ over the visible spectrum from 400 to 900 nm. For a constant pore diameter $D=5$ nm, film thickness L was varied between 0.75 μm and 2 μm corresponding to a L/D ratio between 150 and 400. Fig. 3 shows the retrieved effective index of refraction n_{eff} and the effective absorption index k_{eff} as a function of porosity ϕ for the imaginary nanoporous thin films previously described. A numerically converged solution was obtained with more than 50,000 triangular meshes for 250 wavelengths with a 2 nm increment. The maximum difference in n_{eff} and k_{eff} for $L/D=300$ and $L/D=400$ were 9.9×10^{-3}% and 0.9%, respectively. Thus, the effective optical properties n_{eff} and k_{eff} are independent of L/D as previously observed for TE waves [39,41].

Moreover, the effect of pore diameter D on the effective complex index of refraction was investigated for the same

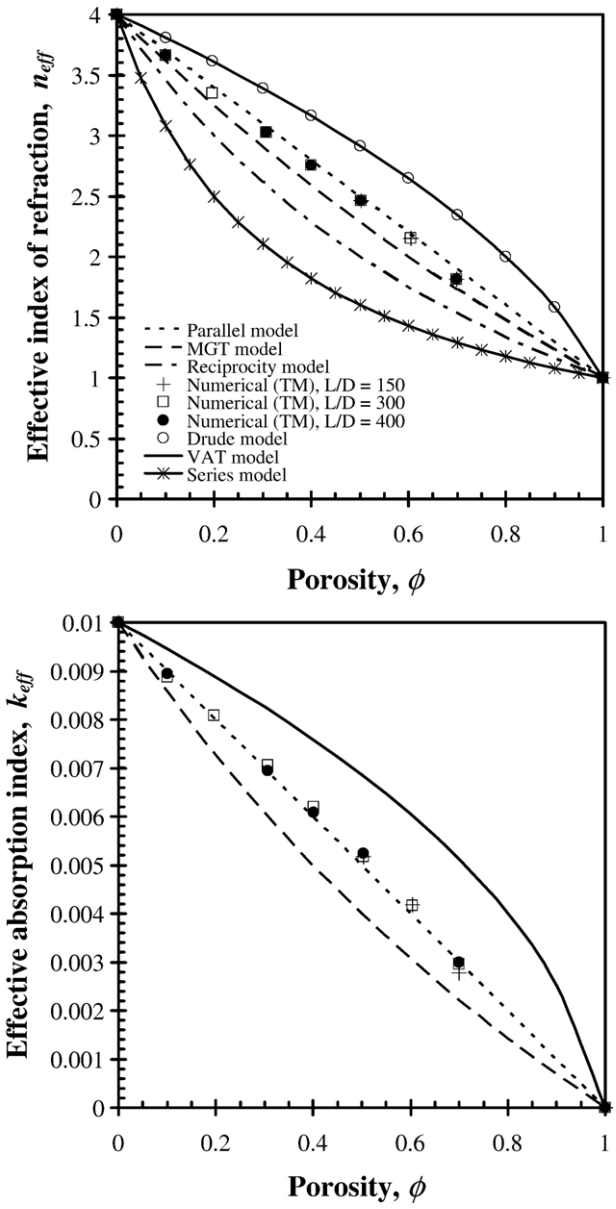

Fig. 3. Effective complex index of refraction as a function of porosity for TM waves incident on thin films with $n_c=4.0$, $k_c=0.01$, $n_d=1.0$, $k_d=0$, $D=5$ nm, $L/D=150$, 300, and 400.

imaginary nanoporous thin film defined in the previous paragraph by holding L/D and ϕ fixed at 400 and 0.1, respectively, while varying pore diameter D between 1 and 10 nm. For D equal to 1, 5, and 10 nm, the recovered effective index of refraction n_{eff} was 3.6361, 3.6624, and 3.6406, respectively while the recovered effective absorption index k_{eff} was 0.0090, 0.0089, and 0.0088, respectively. This corresponds to a maximum relative error in the retrieved n_{eff} and k_{eff} of 0.7% and 2.7%, respectively. Therefore, the effective optical properties are considered to be independent of both the pore diameter and the film thickness for D between 1 and 10 nm and $L/D\geq300$.

Furthermore, the above imaginary nanoporous thin films were examined to assess the validity of the various EMA for TM waves. With a continuous phase index of refraction $n_c=4.0$,

the relative difference between the various effective medium models for n_{eff} and k_{eff} can reach up to 46.0% and 72.7%, respectively. This large difference allows for closer examination and validation of the effective medium models for TM waves. Fig. 3 establishes that the numerical predictions for n_{eff} and k_{eff} agree well with the parallel model predicting $n_{eff}=\phi n_d+(1-\phi)n_c$ and $k_{eff}=\phi k_d+(1-\phi)k_c$. Indeed, the maximum relative error between the numerical results and the predictions from the parallel model for n_{eff} and k_{eff} was 4.3% and 1.6%, respectively. The VAT and the Drude model overpredict the numerical results while the MGT, reciprocity, and series models underpredict them.

Finally, applying the VAT to Maxwell's equations in two-phase media introduces additional surface integral terms in the volume averaged Maxwell's equations [38]. One can treat a heterogeneous medium as homogeneous and solve the Maxwell's equations for a single phase medium with some effective properties only when these additional terms are negligible, i.e., when the electric, magnetic, and electrodynamic equilibria conditions are satisfied concurrently [37,38]. Magnetic equilibrium is always satisfied for non-magnetic materials while electric equilibrium is satisfied for dielectric materials. For TE waves, the surface integral terms (Eqs. (22) to (29) in Ref.[38]) either vanish or cancel each other thanks to the orientation of the electric and magnetic fields with respect to the normal vector of the interfaces between the continuous and dispersed phases. Therefore, the VAT is always valid for TE waves traveling through non-magnetic nanocomposite materials [38]. However, for TM waves, electrodynamic equilibrium is not satisfied and thus the VAT model is not valid.

3.2. Comparison between TM and TE waves

Having established in the previous section that the effective index of refraction n_{eff} and the effective absorption index k_{eff} are independent of pore diameter D and of film thickness L over the given range of L/D, comparisons between TM and TE waves can now be made. Previously, TE waves were simulated for absorbing nanoporous thin films for various porosities, film thicknesses, pore sizes, and arrangements [39]. The present study investigates the same thin films exposed to TM wave as opposed to TE wave. Here also, the continuous phase is defined with constant $n_c=1.44$ and $k_c=0.01$ over the spectral range from 400 to 900 nm while $n_d=n_1=1.0$, $k_d=k_1=k_3=0$, and $n_3=3.39$. Porosity ϕ varies from 0 to 0.7 for a given pore diameter by altering the cubic cell dimensions. In all cases, a numerically converged solution was obtained with more than 50,000 triangular meshes for 250 wavelengths between 400 and 900 nm. Fig. 4 compares the effective index of refraction n_{eff} and absorption index k_{eff} for TM waves with various effective medium models and previous results obtained for incident TE waves [39] as a function of porosity ϕ. The series and reciprocity models are excluded for the effective absorption index k_{eff} since $k_d=0$. As expected, n_{eff} and k_{eff} decrease with increasing porosity. Results from Ref.[39] shows that the VAT model agrees well with the numerical results for TE waves. For TM waves, the maximum relative error between the numerical results and the predictions from the parallel model for n_{eff} and

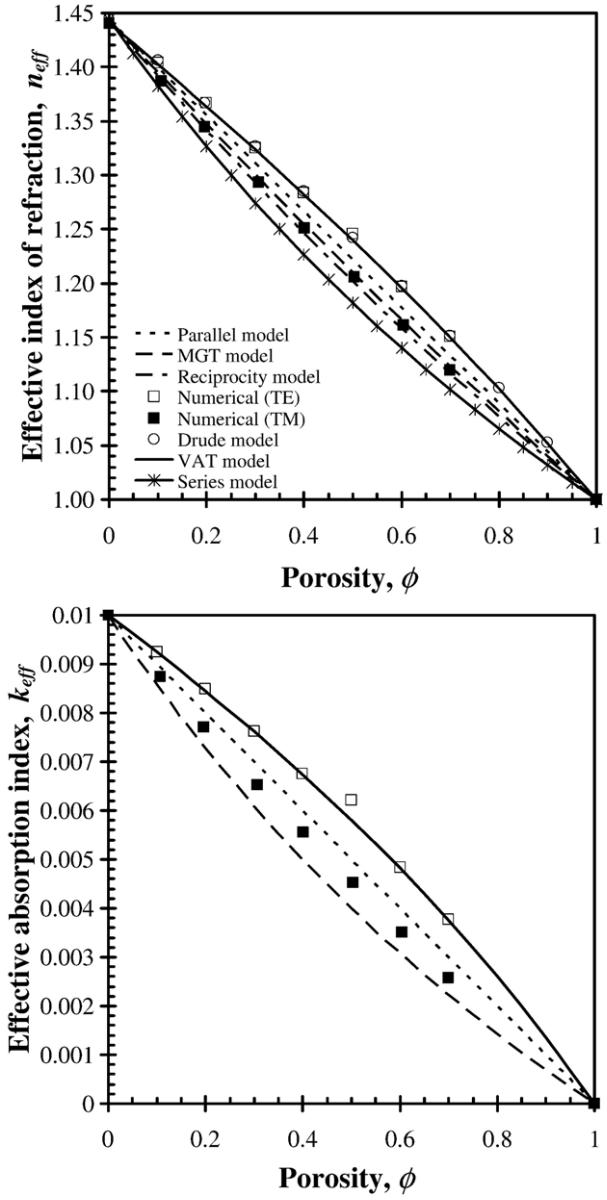

Fig. 4. Effective complex index of refraction as a function of porosity for TE [39] and TM waves incident on nanoporous thin films with $n_c=1.44$, $k_c=0.01$, $n_d=1.0$, $k_d=0$, $D=10$ nm, and $L/D=300$.

k_{eff} was 1.4% and 14.3%, respectively. It is also worth noticing that the maximum difference between the different models is only 4.7% for n_{eff} and 49.6% for k_{eff}. Thus, the parallel model gives good predictions for TM waves. However, unlike the case illustrated in Fig. 3, the MGT and reciprocity models appear also acceptable for n_{eff}. For this reason, an imaginary thin film with a higher continuous phase index of refraction $n_c=4.0$ was chosen in Section 3.1 in order to increase the maximum difference between the effective medium models and identify the best model for TM waves.

3.3. Effect of anisotropy on effective optical properties

In order to study the effect of pore spatial arrangement on effective optical properties, thin films with anisotropic

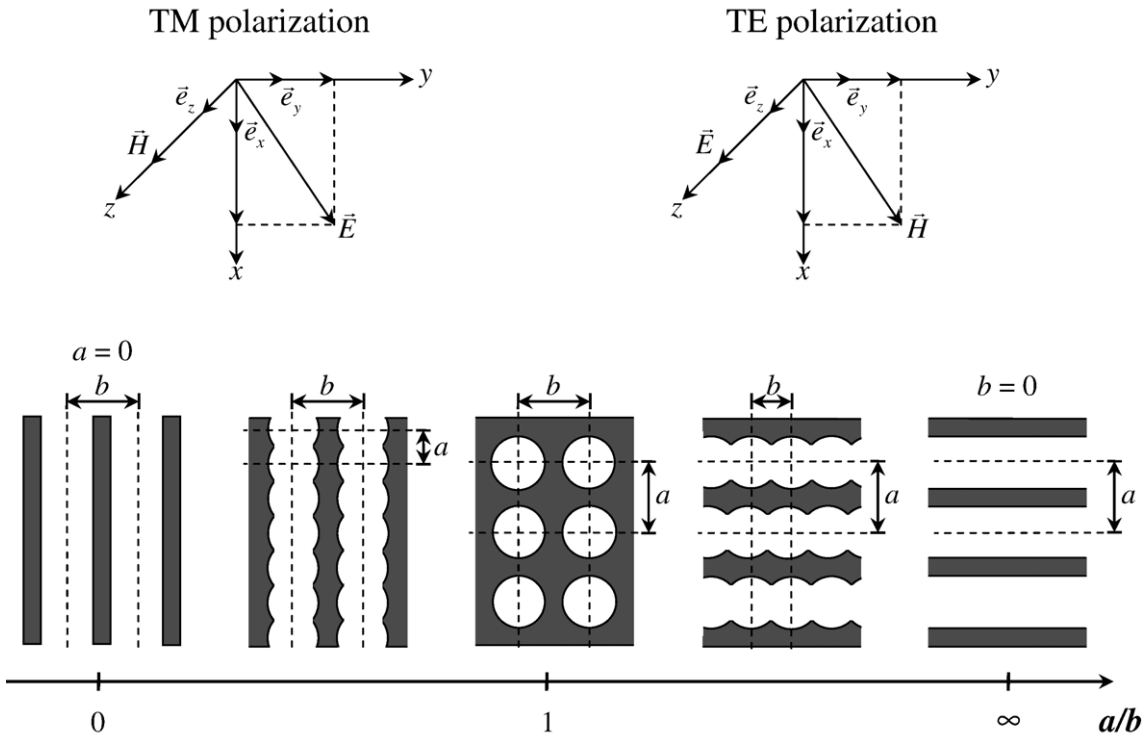

Fig. 5. Absorbing anisotropic nanoporous thin films with various 2D cross sections where a and b refer to the vertical and horizontal distance between pores, respectively.

morphology were examined by varying the distance between pores in the x-and y-directions (see Fig. 2). Fig. 5 illustrates the physical model of absorbing nanocomposite thin films with anisotropic morphology and various aspect ratios a/b where a and b refer to the vertical and horizontal distance between pores, respectively. Note that $a/b=1$ corresponds to a thin film of isotropic morphology where the distance between pores is the same in all directions. For optically anisotropic thin films, the index of refraction and absorption index in the principle directions i.e., $n_{\mathrm{eff,x}}$, $n_{\mathrm{eff,y}}$, $n_{\mathrm{eff,z}}$, $k_{\mathrm{eff,x}}$, $k_{\mathrm{eff,y}}$, and $k_{\mathrm{eff,z}}$, can be determined from the theory presented by Heavens [45] (pp. 92–95). Applying this theory to a non-absorbing thin film with $a/b=0.4$, $n_c=4.0$, $n_d=1.0$, $k_c=k_d=0$, $D=5$ nm, $L/D=300$, and $\phi=0.4$ returns values for $n_{\mathrm{eff,x}}$, $n_{\mathrm{eff,y}}$, and $n_{\mathrm{eff,z}}$ within 0.6% of each other and within 0.3% of n_{eff} predicted for an isotropic thin film. These results justify characterizing heterogeneous thin films with anisotropic morphology consisting of small pores as optically isotropic and homogeneous with some effective optical properties. Thus, the retrieval method previously described can be employed.

Fig. 6 shows the effective index of refraction n_{eff} and the effective absorption index k_{eff} as functions of aspect ratio a/b for both TE and TM waves incident on the nanoporous thin films depicted in Fig. 5 and constant porosity ϕ of 0.4. The solid vertical lines at $a/b=0.51$ and $a/b=1.96$ correspond to lower and upper bounds of thin films with closed pores. For a/b outside this interval, pores intersect with one another and are no longer closed. Here also, a numerically converged solution was obtained with more than 50,000 triangular meshes for 250 wavelengths with a 2 nm increment.

For TE waves, the maximum differences for the retrieved effective index of refraction n_{eff} and the effective absorption index k_{eff} are 0.22% and 0.11%, respectively as a/b varies from zero to infinity. Furthermore, the relative errors between the numerical data and the VAT model for n_{eff} and k_{eff} are 0.65% and 1.0%, respectively. The small variations in n_{eff} and k_{eff} can be attributed to numerical uncertainties in the values of T_{num} and R_{num} and in the retrieval method. In brief, for TE polarization, the effective optical properties are independent of the pore spatial arrangement. They depend only on porosity and are in good agreement with the VAT model. This can be attributed to the fact that the normal vector of all cylindrical pores simulated (see Fig. 2) is confined to the x–y plane and is always perpendicular to the electric field of a TE polarized plane wave, i.e., $\vec{E}=E_z\vec{e}_z$. Thus, polarization has no effect on reflection and refraction across the interface.

In contrast, for TM waves, the effective index of refraction n_{eff} and the effective absorption index k_{eff} increase with increasing a/b. As a/b goes to infinity, n_{eff} and k_{eff} converge to the numerical values found for TE polarization which matches the VAT model predictions. Indeed, as a/b tends to infinity, the morphology of the thin film approaches that of a superlattice consisting of alternating thin films of continuous and dispersed phases for which the normal vectors of all interfaces are collinear with the Poynting vector. Then, the plane of incidence and thus, the polarization cannot be defined. However, for a/b ratios other than infinity, the normal vector of the continuous-dispersed interfaces is not collinear to the Poynting vector at all points around the cylindrical pores. Thus, while the nanoporous thin film can be treated as optically

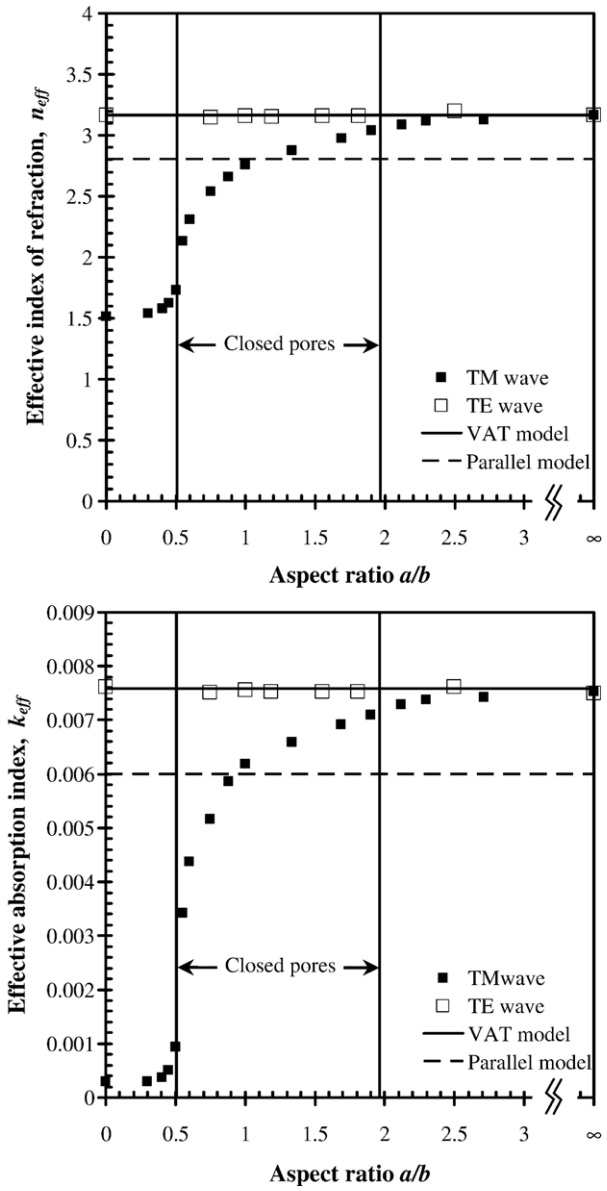

Fig. 6. Effective complex index of refraction as a function of aspect ratio (a/b) for TE and TM waves incident on thin films with n_c=4.0, k_c=0.01, n_d=1.0, k_d=0, D=5 nm, ϕ=0.4, and L/D=300.

isotropic and homogeneous, the presence of an interface and the morphology causes different behavior for TE and TM polarizations. This is not observed for dense thin films as previously discussed and as observed numerically. Finally, when a/b=0, none of the effective medium models predict the effective optical properties.

Finally, this study shows that the effective optical properties of nanocomposite thin films can be tuned by changing not only the porosity but also the pore spatial arrangement. The relatively steep slope in Fig. 6 for n_{eff} and k_{eff} for a/b between 0.4 and 2.0 also indicates that small changes in pore spatial distribution lead to large changes in the effective optical properties. Thus, measuring the transmittance and reflectance of nanocomposite materials for TM waves can provide a non-invasive optical method to determine their morphology. Simultaneously, TE waves can be used to measure the film porosity. This can also explain or reconcile discrepancies in the experimental data reported in the literature and reaching contradictory conclusions regarding the validity of EMA [46].

4. Conclusions

This paper numerically assesses the effect of porosity and pore shape, size, and spatial distribution on the effective optical properties of nanocomposite thin films exposed to TM or TE waves. Porosity was varied from 0 to 0.7 and pore diameter between 1 and 10 nm. Finally, thin films with anisotropic morphologies were examined by varying the interpore distances in the plane of incidence. The effective complex index of refraction $m_{eff}=n_{eff}-ik_{eff}$ was retrieved from the transmittance and reflectance computed from the time-harmonic field solution of Maxwell's equations over the spectrum between 400 nm and 900 nm. The effective index of refraction n_{eff} and the effective absorption index k_{eff} were determined to be independent of pore diameter D and film thickness L for $L/D \geq 300$. For TE incident waves, n_{eff} and k_{eff} depend only on porosity and good agreement was found with predictions from the VAT model [39]. For TM waves, the effective optical properties depend on both pore spatial arrangement and porosity. For equally spaced pores, both n_{eff} and k_{eff} for TM waves are in good agreement with predictions from the parallel model. These results extend our previous studies [39] from TE to TM polarizations and serve in the design of nanocomposite materials with tunable optical properties. Finally, they also indicate that the film porosity could be measured from transmittance and reflectance data for TE waves while the morphology could be retrieved from TM wave measurements.

Nomenclature

A	Dimensionless parameter, Eq. (8)
a	Distance between pores in the y-direction
B	Dimensionless parameter, Eq. (9)
b	Distance between pores in the x-direction
c	Speed of light
D	Pore diameter
$\vec{E}$	Electric field vector
$\vec{e}$	Unit vector
$\vec{H}$	Magnetic field vector
k	Absorption index
L	Thickness of the thin film
m	Complex index of refraction, $m = n - ik$
n	Real part of complex index of refraction
$\vec{n}$	Normal vector
N	Number of wavelengths considered
Q	Efficiency factor
R	Reflectance
r	Interface reflectivity
T	Transmittance
t	Time
W	Cubic cell width
x, y, z	Spatial coordinates

Greek symbols

χ	Size parameter
δ	Phase angle
ε	Dielectric constant
ϕ	Porosity
κ	Absorption coefficient
λ	Wavelength
μ	Magnetic permeability
$\vec{\pi}$	Poynting vector
σ	Electrical conductivity
τ	Interface transmissivity
ω	Angular frequency
ψ	General property
ζ	Dimensionless parameter, Eq. (20)

Subscripts

0	Refers to vacuum, or an incident wave
1	Refers to surroundings in thin-film system
2	Refers to thin-film
3	Refers to substrate
abs	Refers to absorption
avg	Refers to time averaged value
c	Refers to continuous phase
d	Refers to dispersed phase
eff	refers to effective property
i	Refers to medium *i* or summation index
j	Refers to medium *j* or summation index
max	Refers to a maximum value
num	Refers to numerical result
r	Refers to relative property
sca	Refers to scattering
th	Refers to theoretical calculation
x	Refers to *x*-direction
y	Refers to *y*-direction
z	Refers to *z*-direction

Acknowledgements

The authors thank Soojung Claire Hur for synthesizing and providing the transmission electron microscopy (TEM) image of hexagonal mesoporous silica thin films shown in Fig. 1. This material is based upon work supported in part by the National Science Foundation under Grant No. CTS-0449429.

References

[1] C.J. Brinker, Y. Lu, A. Sellinger, H. Fan, Adv. Mater. 11 (1999) 579.
[2] H. Fan, H.R. Bentley, K.R. Kathan, P. Clem, Y. Lu, C.J. Brinker, J. Non-Cryst. Solids 285 (2001) 79.
[3] P.C.A. Alberius, K.L. Frindell, R.C. Hayward, E.J. Kramer, G.D. Stucky, B.F. Chmelka, Chem. Mater. 14 (2002) 3284.
[4] B.W. Eggiman, M.P. Tate, H.W. Hillhouse, Chem. Mater. 18 (2006) 723.
[5] B. O'Regan, M. Grätzel, Nature 353 (1991) 737.
[6] P. Ravirajan, S.A. Haque, D. Poplavskyy, J.R. Durrant, D.D.C. Bradley, J. Nelson, Thin Solid Films 451 (2004) 624.
[7] L. Schmidt-Mende, M. Grätzel, Thin Solid Films 500 (2006) 296.
[8] M.I. Sanchez, J.L. Hedrick, T.P. Russell, J. Polym. Sci., Part B, Polym. Phys. 33 (1995) 253.
[9] M.I. Sanchez, J.L. Hedrick, T.P. Russell, Microporous and macroporous materials, Materials Research Society Symposium Proceedings, 431, Materials Research Society, Pittsburgh, PA, U.S.A., 1996, p. 475.
[10] F. Cernuschi, S. Ahmaniemi, P. Vuoristo, T. Mantyla, J. Eur. Ceram. Soc. 24 (2004) 2657.
[11] Q. Hu, R. Kou, J. Pang, T.L. Ward, M. Cai, Z. Yang, Y. Lu, J. Tang, Chem. Commun. 6 (2007) 601.
[12] R.J. Martin-Palma, V. Torres-Costa, M. Arroyo-Hernandez, M. Manso, J. Perez-Rigueiro, J.M. Martinez-Duart, Microelectron. J. 35 (2004) 45.
[13] M. Arroyo-Hernandez, R.J. Martin-Palma, J. Perez-Rigueiro, J.P. Garcia-Ruiz, J.L. Garcia-Fierro, J.M. Martinez-Duart, Mater. Sci. Eng. 23 (2003) 697.
[14] S. Chan, Y. Li, L.J. Rothberg, B.L. Miller, P.M. Fauchet, Mater. Sci. Eng. 15 (2001) 277.
[15] A. Loni, L.T. Canham, M.G. Berger, R. Arens-Fischer, H. Munder, H. Luth, H.F. Arrand, T.M. Benson, Thin Solid Films 276 (1996) 143.
[16] H.F. Arrand, T.M. Benson, A. Loni, M.G. Krueger, M. Thoenissen, H. Lueth, Electron. Lett. 33 (1997) 1724.
[17] A. Jain, S. Rogojevic, S. Ponoth, I. Matthew, W.N. Gill, P. Persans, M. Tomozawa, J.L. Plawsky, E. Simonyi, Thin Solid Films 398 (2001) 513.
[18] M.G. Berger, M. Thonissen, R. Arens-Fischer, H. Munder, H. Luth, M. Arntzen, W. Thei, Thin Solid Films 255 (1995) 313.
[19] J. Diener, N. Künzner, D. Kovalev, E. Gross, V.Y. Timoshenko, G. Polisski, F. Koch, Appl. Phys. Lett. 78 (2001) 3887.
[20] M. Krüger, M. Marso, M.G. Berger, M. Thönissen, S. Billat, R. Loo, W. Reetz, H. Lüth, S. Hilbrich, R. Arens-Fischer, P. Grosse, Thin Solid Films 297 (1997) 241.
[21] S. Zangooie, M. Schubert, C. Trimble, D.W. Thompson, J.A. Woollam, Appl. Opt. 40 (2001) 906.
[22] S. Zangooie, R. Jansson, H. Arwin, J. Appl. Phys. 86 (1999) 850.
[23] C. Mazzoleni, L. Pavesi, Appl. Phys. Lett. 67 (1995) 2983.
[24] K. Kordás, S. Beke, A.E. Pap, A. Uusimäki, S. Leppävuori, Opt. Mater. 25 (2004) 257.
[25] J.C. Maxwell, Garnett Philos. Trans. R. Soc. Lond. Ser. A: Math. Phys. Sci. 203 (1904) 385.
[26] H.J. Cha, J. Hedrick, R.A. DiPietro, T. Blume, R. Beyers, D.Y. Yoon, Appl. Phys. Lett. 68 (1996) 1930.
[27] B. Krause, G.H. Koops, N.F.A. van der Vegt, M. Wessling, M. Wubbenhorst, J. Van Turnhout, Adv. Mater. 14 (2002) 1041.
[28] S. Labbe-Lavigne, S. Barret, F. Garet, L. Duvillaret, J.L. Coutaz, J. Appl. Phys. 83 (1998) 6007.
[29] C. Himcinschi, M. Friedrich, C. Murray, I. Streiter, S.E. Schulz, T. Gessner, D.R.T. Zahn, Semicond. Sci. Technol. 16 (2001) 806.
[30] O. Yavas, P. Leiderer, H.K. Park, C.P. Grigoropoulos, C.C. Poon, W.P. Leung, N. Do, A.C. Tam, Phys. Rev. Lett. 70 (1993) 1830.
[31] G. Grimvall, Thermophysical Properties of Materials, Selected Topics in Solid State Physics, vol. XVIII, North-Holland Physics Publishing, 1986.
[32] J.J. Si, H. Ono, K. Uchida, S. Nozaki, H. Morisaki, N. Itoh, Appl. Phys. Lett. 79 (2001) 3140.
[33] L.W. Hrubesh, L.E. Keene, V.R. Latorre, J. Mater. Res. 8 (1993) 1736.
[34] E. Kondoh, M.R. Baklanov, E. Lin, D. Gidley, A. Nakashima, Jpn. J. Appl. Phys. 40 (2001) L323.
[35] F.J. Balta Calleja, R.K. Bayer, T.A. Ezquerra, J. Mater. Sci. 23 (1988) 1411.
[36] T.C. Choy, Effective Medium Theory: Principles and Applications, Oxford University Press, New York, 1999.
[37] J.A. del Río, S. Whitaker, Trans. Por. Med. 39 (2000) 159.
[38] J.A. del Río, S. Whitaker, Trans. Por. Med. 39 (2000) 259.
[39] A. Garahan, L. Pilon, J. Appl. Phys. 101 (2007) 014320.
[40] C.C. Lee, C.J. Tang, Appl. Opt. 45 (2006) 9125.
[41] M.M. Braun, L. Pilon, Thin Solid Films 496 (2006) 505.
[42] M.F. Modest, Radiative Heat Transfer, Academic Press, San Diego, CA, 2003.
[43] M.Q. Brewster, Thermal Radiative Transfer and Properties, John Wiley and Sons, Inc., New York, NY, 1992.
[44] J. Yin, L. Pilon, J. Opt. Soc. Am., A. 23 (2006) 2784.
[45] O.S. Heavens, Optical Properties of Thin Solid Films, Dover, New York, NY, 1991.
[46] M.M. Braun, Master's Thesis, Department of Mechanical and Aerospace Engineering, University of California, Los Angeles, CA, 2004.